RESEARCH ARTICLE

NANO · MICRO small
www.small-journal.com

High Polymer Molecular Weight Yields Solar Cells with Simultaneously Improved Performance and Thermal Stability

Sergi Riera-Galindo, Marta Sanz-Lleó, Edgar Gutiérrez-Fernández, Nicolás Ramos, Marta Mas-Torrent, Jaime Martín, Laura López-Mir,* and Mariano Campoy-Quiles**

Simple synthetic routes, high active layer thickness tolerance as well as stable organic solar cells are relentlessly pursued as key enabling traits for the upscaling of organic photovoltaics. Here, the potential to address these issues by tuning donor polymer molecular weight is investigated. Specifically, the focus is on PTQ10, a polymer with low synthetic complexity, with number average molecular weights of 2.4, 6.2, 16.8, 52.9, and 54.4 kDa, in combination with three different non-fullerene acceptors, namely Y6, Y12, and IDIC. Molecular weight, indeed, unlocks a threefold increase in power conversion efficiency for these blends. Importantly, efficiencies above 10% for blade coated devices with thicknesses between 200 and 350 nm for blends incorporating high molecular weight donor are shown. Spectroscopic, GIWAXS and charge carrier mobility data suggest that the strong photocurrent improvement with molecular weight is related to both, improved electronic transport and polymer contribution to exciton generation. Moreover, it is demonstrated that solar cells based on high molecular weight PTQ10 are more thermally stable due to a higher glass transition temperature, thus also improving device stability.

1. Introduction

Organic photovoltaics (OPVs) can be a competitive player in the photovoltaic solar energy industry in applications such as wearable electronics, indoor photovoltaics, building integrated photovoltaics, or agrivoltaics.[1–4] The recent progress in OPV technology has been mainly triggered by the important advances in the development of new photoactive semiconductor organic materials, especially non-fullerene acceptor molecules (NFAs) and tuned band gap donor polymers,3 which have led to an impressive performance increase with power conversion efficiencies (PCEs) in lab-scale single junction devices exceeding 19%.[5–11] Despite the advent of OPV active materials with high efficiency,[12–16] the mass adoption of solution processed OPV is still hindered by a few scientific and engineering challenges, mainly in terms of upscaling, costs, and stability.[17–21] While it is of paramount importance for successful commercialization of NFA-based OPV modules, the research community has not paid enough attention to stability so far, focusing its efforts on improving PCEs.

In particular, thermal stability is one of the key challenges facing the widespread adoption of organic solar cells.[22] Thermal stability refers to the ability of the device to maintain its performance under operational (or elevated) temperatures. Qualification standard tests for photovoltaics such as IEC 61215 and IEC 61646, take this very important feature into account by exposing the modules under test to repeated temperature cycles from −40 °C to +80 °C. Conjugated polymers and small organic molecules can have low thermal stability and thus be prone to degradation under moderate or high temperature excursions.

Exposing an OPV cell to high temperatures can lead to several degradation routes. The most prevalent is related to bulk heterojunction (BHJ) evolution as a consequence of molecular diffusion and aggregation/crystallization tendency which results in donor/acceptor phase separation.[23–25] Besides, temperature may promote ion migration and, generally, the degradation of the interfaces between the various components of the device.[26] Finally, exposing the device to high temperatures can accelerate, in combination with other agents such as oxygen, the chemical

S. Riera-Galindo, M. Sanz-Lleó, M. Mas-Torrent, M. Campoy-Quiles
Institute of Materials Science of Barcelona ICMAB-CSIC
Campus Universitat Autònoma de Barcelona (UAB)
Bellaterra 08193, Barcelona, Spain
E-mail: sriera@icmab.es; mcampoy@icmab.es

M. Sanz-Lleó, L. López-Mir
Eurecat Centre Tecnològic de Catalunya
Unit of Printed Electronics & Embedded Devices
Av. d'Ernest Lluch 36, Mataró 08302, Spain
E-mail: laura.lopezm@eurecat.org

E. Gutiérrez-Fernández, N. Ramos, J. Martín
POLYMAT and Polymer Science and Technology Department
Faculty of Chemistry
University of the Basque Country UPV/EHU
Donostia-San Sebastián 20018, Spain

J. Martín
Universidade da Coruña
Campus Industrial de Ferrol
CITENI, Esteiro, Ferrol 15403, Spain

The ORCID identification number(s) for the author(s) of this article can be found under https://doi.org/10.1002/smll.202311735

DOI: 10.1002/smll.202311735

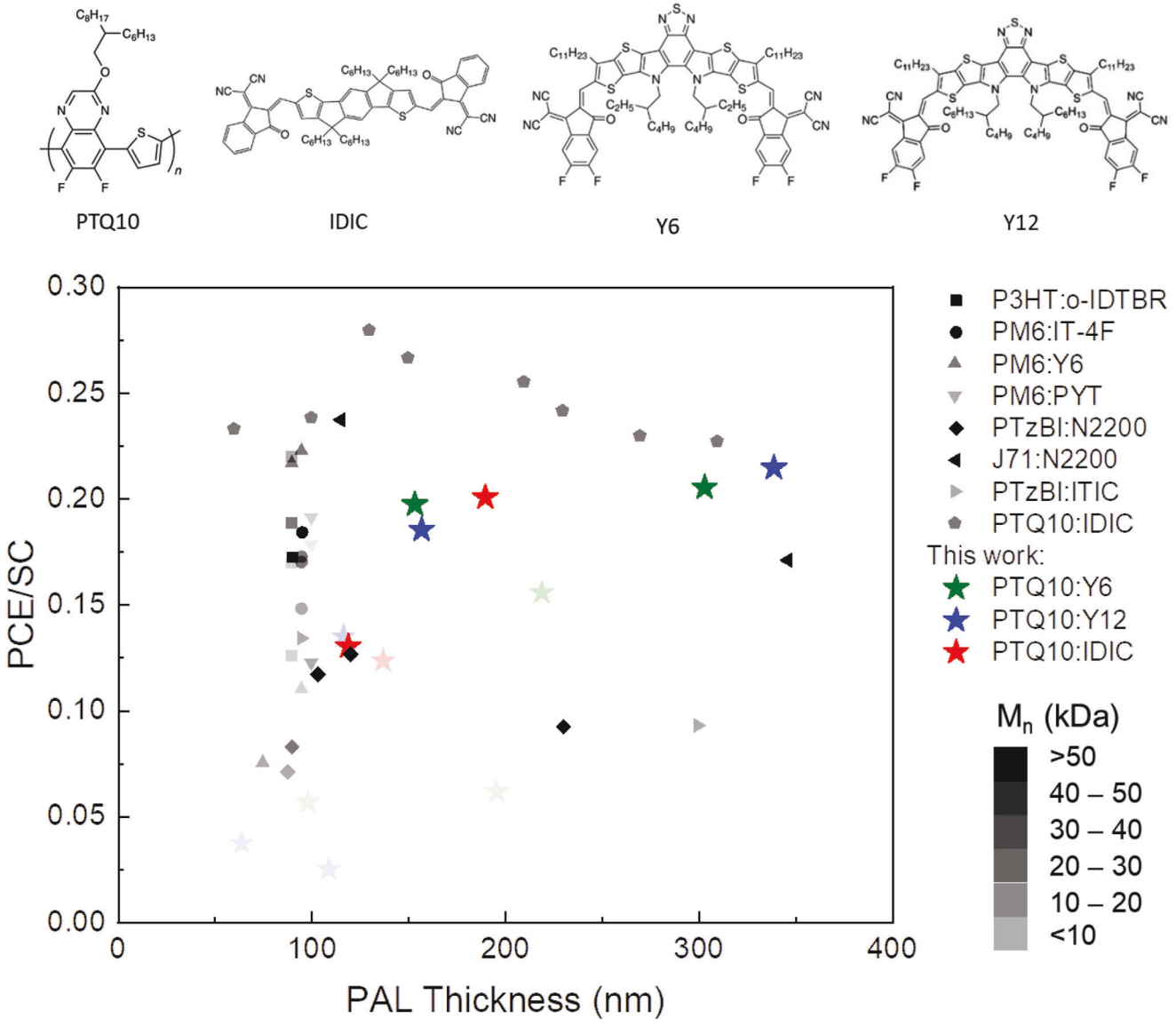

Figure 1. Top: Molecular structures of the organic semiconductors used in this work. Bottom: Power conversion efficiency (PCE, %) to synthetic complexity (SC, %) ratio as a function of active layer thickness with different number average molecular weights of the donor polymer for selected combinations reported in the literature: for PM6:IT-4F,[46] PM6:Y6,[45,47] P3HT:o-IDTBR,[48] PTzBI:N2200,[54] PTQ10:IDIC,[60] PM6:PYT,[65] J71:N2200,[66] PTzBI:ITIC.[67]

degradation of the active layer through, for example chain scission, changes in the molecular weight of the materials and defect formation. Related to the above, several geometric and device parameters have been found to influence the thermal stability of an organic solar cell, including the photoactive layer (PAL) thickness,[27] the presence of a third component or stabilizing additives,[28–33] the solvent choice,[34] the use of photocrosslinkable polymers,[35–37] interlayer modification,[38,39] and device architecture.[40]

Importantly, PAL thickness also has a profound effect on PCE as it dictates the amount of light absorbed. While thicker films would improve absorption, the final PCE is limited by electronic transport and doping and thus, a compromise is found with optimum thickness often ≈100 nm.[41] From an upscaling point of view, coating large areas at exactly 100 nm is extremely challenging, so materials and geometries that exhibit a performance that is resilient to changes in thickness are of great interest.

On the other hand, the molecular weight (M_n) has a significant impact on the device performance,[42] as it has been reported in organic electrochemical transistors,[43] thermoelectric devices,[44] organic light emitting diodes,[45] and organic photovoltaics (see **Figure 1**). Increasing the molecular weight of polymers generally enhances their film-forming properties; nonetheless, processing high molecular weight polymers is challenging due to their limited solubility. In recent developments, a high-pressure method has been employed for processing high molecular weight D18, enabling the achievement of an exceptional power conversion efficiency of 19.65%.[11] This achievement sets

a new record for binary devices to date. Moreover, high molecular weight polymers achieve higher charge carrier mobility, offering a higher device performance. In OPVs, the general observation is that higher M_n improves PCE. This has been shown for different OPV systems, including those based on P3HT, PTB7-Th, TQ-F, PTzBi, and PM6 donors (Figure 1) blended with a number of acceptors. Other works on polymer:fullerene follow the same M_n-dependence.[46] For the sake of clarity we have focus on the collection of data related to polymer:NFAs and polymer:polymer systems. While there has been efforts to determine the most critical molecular-weight sensitive factors impacting OPV performance, a general framework for device optimization is, however, still missing.[46] Some works carefully identify bulk and interfacial morphological factors affecting charge extraction and transport in OPV.[46–49] A considerable amount of research has been devoted to show the importance of controlling the M_n of the donor polymer on BHJ OPVs for maximizing device performance and reproducibility.[46–59] The improved performance can be attributed to several factors, including higher light absorption, improved charge transport, and reduced aggregation and phase separation of the polymer chains. Moreover, it is expected that high M_n donor polymers show high thermal stability;[52] since the higher M_n can reduce chain dynamics of the polymer, thus increasing the glass transition temperature and, in consequence, reducing the potential phase segregation.

In the present work, we have shed light into the molecular weight dependence of BHJ based on NFAs combined with poly[[6,7-difluoro[(2-hexyldecyl)oxy]−5,8-quinoxalinediyl]−2,5-thiophenediyl] (PTQ10), a high performance polymer donor material used in current state-of-the-art OPV research. PTQ10 has a simple molecular structure and can be synthesized through a streamlined two-step process making it a highly versatile and low cost material which bright future for commercialization.[60] Recently, PTQ10 has been documented to exhibit superior photostability compared to benchmark donor polymers PM6 and D18, which has been attributed to the increased planarity and rigidity in PTQ10 backbone structure.[61] Three different NFAs molecules have been chosen for the study: 2, 2′- [(4,4,9,9-Tetrahexyl – 4, 9- dihydro-s- indaceno [1,2-b:5,6-b′] – dithiophene – 2,7-diyl) bis [methylidyne (3- oxo – 1H – indene – 2,1 (3H) – diylidene)]] bis – propanedinitrile (IDIC) or Y-family (like 2,2″-((2Z,2″Z)-((12,13-bis(2-ethylhexyl)−3,9-diundecyl-12,13-dihydro-[1,2,5]thiadiazolo [3,4 – e] thieno [2″, 3″: 4′, 5′] thieno [2′, 3′: 4, 5] pyrrolo [3, 2 – g] thieno [2′, 3′ :4, 5] thieno [3, 2 – b] indole – 2, 10 – diyl) bis (methanylylidene)) bis (5, 6 – difluoro – 3 – oxo – 2, 3 – dihydro – 1H – indene – 2, 1 – diylidene)) dimalononitrile (Y6) and 2, 2′ – ((2Z, 2″Z) – ((12, 13 – bis (2 – butyloctyl) – 3, 9 -diundecyl – 12, 13 – dihydro – [1, 2, 5] thiadiazolo [3, 4 – e] thieno [2″, 3″: 4′, 5′] thieno [2′, 3′: 4, 5] pyrrolo [3, 2 – g] thieno [2′, 3′: 4, 5] thieno [3, 2 – b] indole – 2, 10 – diyl) bis (methanylylidene)) bis (5, 6 – difluoro – 3 – oxo – 2, 3 – dihydro – 1H – indene – 2, 1 – diylidene)) dimalononitrile (Y12)).[62] PTQ10:IDIC blend has shown an apparent low dependence to active layer thickness.[63] Y6 and its derivates, such as Y12, with increased solubility with non-halogenated solvents,[64] are the nowadays benchmark acceptors. Still, there are no studies of the molecular weight dependence of the photovoltaic performance on PTQ10:NFA based solar cells.

In this work, we explore the effect of molecular weight on PTQ10-based OPV. Five different PTQ10 with number average molecular weights (M_n) ranging from low (≈2.4 and ≈6.2 kDa), medium (≈16.8 kDa), and high (≈52.9 and ∼54.4 kDa) molar mass fractions have been tested by combinatorial screening with the aforementioned three NFAs, namely IDIC, Y6 and Y12. The active layer materials have been analysed by measuring their charge carrier mobility, absorption, grazing-incidence wide-angle x-ray scattering (GIWAXS), Raman, and differential scanning calorimetry (DSC).

The presented results shed light on a practical processing route for scaling up PTQ10:NFA-based OPV using high M_n PTQ10 and thicker photoactive layers. Notably, the adoption of higher molecular weight polymers does not only lead to improved device performance but also yields greater PAL thickness tolerance and thermal stability, which are crucial aspects for the commercialization of OPV. Additionally, it is imperative to consider the intricacy involved in synthesizing the raw materials. The concept of synthetic complexity (SC) is designed to quantify the experimental effort necessary for manufacturing organic semiconducting materials for use in OPV,[68] which we view as a proxy for the cost associated with these materials. Simultaneously obtaining these aspects is extremely challenging. Figure 1 shows that the PCE to SC ratio as a function of PAL thickness, where we include prior studies to optimize the PAL thickness and other works about the M_n of the donor polymer. Our high-throughput fabrication approach enables us to conduct these tasks effortlessly. The quadrant with high PCE/SC ratio and high PAL thickness is hardly populated, being the results here presented significant in this respect. Overall, this research demonstrates the importance of incorporating higher M_n donor polymer in PTQ10:NFA-based OPV, paving the way for more efficient and stable solar energy conversion technologies.

2. Results and Discussion

In a first series of experiments, we fabricated devices based on PTQ10:NFA systems with an inverted structure (ITO/ZnO/PTQ10:NFA/MoO_x/Ag) with different PTQ10 M_n and using three different NFAs, namely IDIC, Y6 and Y12, supplementary details about the properties of the PTQ10 polymers utilized in this study can be find in Table S1 (Supporting Information). These sum up to 13 different blend combinations and a total of 312 devices. In order to minimize the required amount of material and simultaneously accelerate the screening process, we employed a recently developed high throughput screening method.[69–71] Specifically, we deposited the corresponding PALs as thickness gradients via decelerating blade coating. This process defined 12 pixels of varying thickness on each substrate, facilitating a rapid and material-efficient optimization of the PAL thickness dependency. The method involved testing 12 distinct parametric combinations, each replicated twice, resulting in a total of 24 devices or pixels arranged in a single large aspect ratio (see Figure S1, Supporting Information and Video in Ref.[72]). The PAL thickness variation of the along the substrate significantly influences the final power conversion efficiency (PCE).

The main photovoltaic parameters of all the PTQ10:NFA systems as a function of thickness and for each M_n are shown in

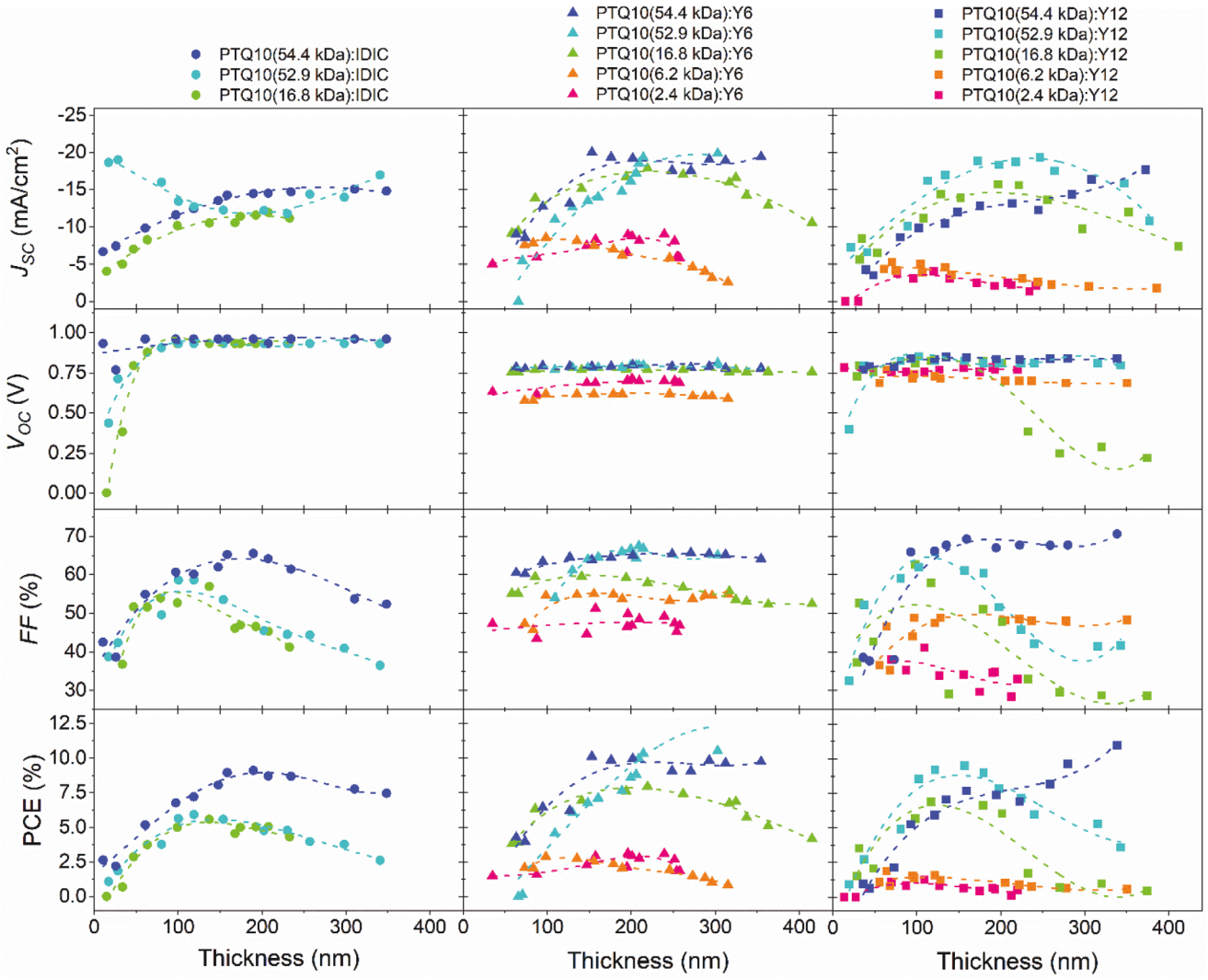

Figure 2. Main photovoltaic parameters as a function of PAL thickness for OPVs based on PTQ10:NFA with different M_n of PTQ10, using as NFA: IDIC (left column), Y6 (middle column), and Y12 (right column). Dashed lines are polynomial fitting to the data, acting as visual guidelines.

Figure 2. The *J(V)* of the champion device for each NFA are depicted in Figure S2 (Supporting Information). Overall, the performance improves with increasing M_n in all cases. We can attribute the improvement in PCE due to the increase in J_{SC} and *FF* for blends containing higher M_n PTQ10. For a given material system, the open circuit voltage remains fairly constant as a function of both thickness and polymer M_n. The higher V_{OC} obtained for IDIC acceptor ($V_{OC,max}$ = 0.96 V) compared to those using Y6 or Y12 acceptors ($V_{OC,max}$ = 0.79 and 0.86 V, respectively) can be attributed to its higher lying lowest unoccupied molecular orbital (LUMO)(−3.91 eV)[73] than the LUMO level of Y6 (−4.10 eV)[74] or Y12 (−4.06 eV).[64] Systems with Y6 and Y12 acceptors achieve higher PCEs (> 10%) than the system with IDIC as a result of higher J_{SC} values (attributed to the broader absorption of Y6 and Y12, see **Figure 3**) and slightly better *FF*, which can indicate a better charge transport in Y6 and Y12 systems, as shown below. In the case of the PTQ10:Y6 devices, the PCE increases from 3.1% (M_n of PTQ10 2.4 kDa) to 10.1% (M_n of PTQ10 54.4 kDa), which represents a threefold increase in PCE.

Interesting, the optimum thickness for the PTQ10:NFA-based OPV is relatively high, achieving the highest PCE of 9.1%, 10.5%, and 11% at 190, 302, and 339 nm, when combining high molecular weight PTQ10 with IDIC, Y6, and Y12, respectively (Figure 2). The thickness that maximizes PCE increases with M_n, which points toward transport issues for lower molecular weights. Reassuringly, the good *FF* values (> 65%) obtained for PAL thicker than 150 nm and high M_n indicates low recombination and transport losses.[41] High *FF*s and J_{SC} values are in agreement with lower density of recombination centres and better photoactive layer morphology in the samples with higher M_n (Figure S3, Supporting Information)[52] as well as better transport properties and complementary absorption (see below).

Another aspect related to the thickness dependence is how much does the PCE varies with small changes in thickness, what is normally referred to as thickness tolerance. Previously, high tolerance to PAL thickness was reported using also PTQ10 as donor polymer blended with either IDIC or fullerene.[60,75] In the present study, OPV performance based on PTQ10:IDIC shows

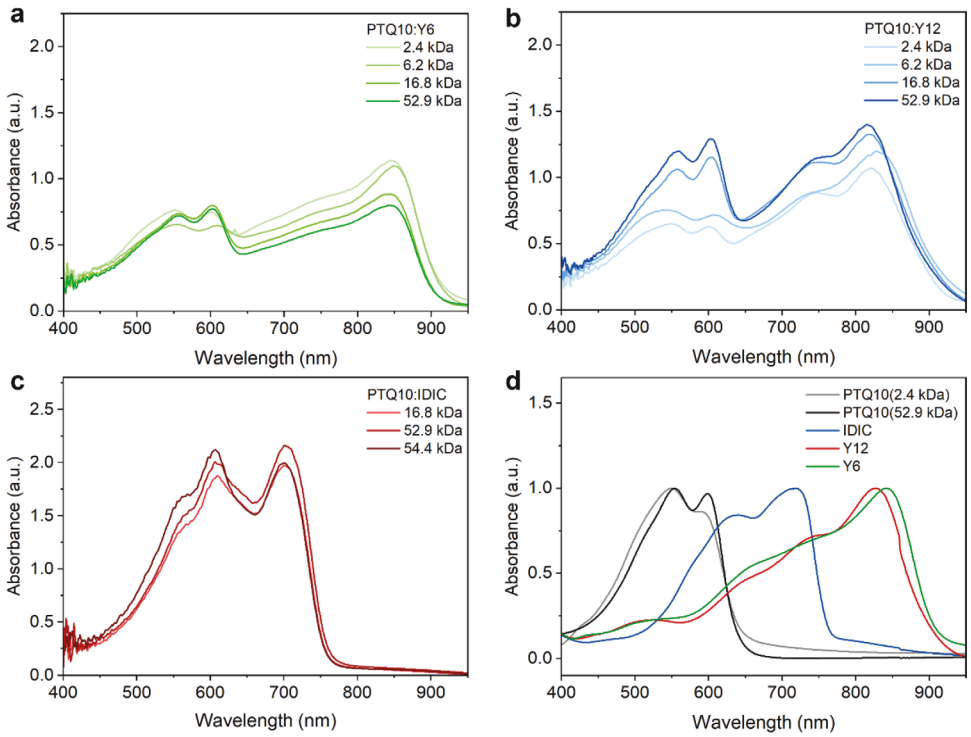

Figure 3. Absorption spectra of PTQ10:NFA blends with similar thickness ≈200 nm and different M_n of PTQ10 a–c) and normalized absorption spectra for neat materials (PTQ10(2.4 kDa), PTQ10(52.9 kDa), IDIC, Y12 and Y6) d).

very low dependence on PAL thickness above a certain threshold, in good agreement with previous reports.[63] For Y6 and Y12 based devices, we demonstrate also broad thickness tolerance. In all cases, how flat is the PCE versus thickness (for thickness above 100 nm) is strongly dependent on molecular weight, generally becoming more thickness insensitive for high M_n.

The results presented reveal relevant processing indicators for the scaling up of PTQ10:NFA-based OPV which is the requirement of high molecular weight and thick PAL deposition,[76] since the performance peaks encountered in the studied OPVs are beyond 100 nm in PAL thickness. This is not frequent in OPV for the best performing donor:acceptor combinations reported up to now[75,77–80] and represents a clear advantage of this polymer for solution processing of flexible OPV due to an increased compatibility with upscaling deposition techniques such as slot die coating or screen printing.

In order to understand the differences in device performance as a function of PTQ10 M_n, we have measured UV–vis–NIR absorption and external quantum efficiency (EQE) for the different blends of PTQ10 with the selected NFAs. Figure 3 shows UV–vis absorption measurements on samples of PTQ10:Y6 (a), PTQ10:IDIC (b), PTQ10:Y12 (c), and with similar thickness and different M_n and the neat materials (d). The complete set of absorption spectra of the different combinations can be found in Figure S4 (Supporting Information). PTQ10 absorption bands are centred at ≈600 nm, IDIC at 715 nm, and Y12 and Y6 at ≈825 and 840 nm, respectively. In the case of PTQ10, the spectra of low and high M_n have been plotted for comparison. Depending on the M_n, the absorption of PTQ10 shows different band shape (different relative intensity between the peaks), and sharper for the high M_n case. The absorption band broadening is affected by the conjugation length and the molecular disorder.

With respect to the blends, the narrower absorption spectrum of PTQ10:IDIC films is due to the higher bandgap of IDIC, which is also related to higher V_{OC} shown by the corresponding devices. Ostensibly, PTQ10:IDIC films exhibit higher optical absorption than thin films based on Y-derivates acceptors for a given thickness. One puzzling finding is that, for all the considered systems, when the films contain low M_n PTQ10, the acceptor absorption contribution is higher; however, for high M_n PTQ10, the contributions to absorption from both components absorptions are more compensated. The origin of this is still unclear, and two hypotheses could explain it. A first explanation would be that low M_n PTQ10 exhibit a lower extinction coefficient, either intrinsic due to a smaller oscillator strength[81] or in the plane of the substrate, due to a more isotropic dipole distribution.[82] Alternatively, the actual amount of PTQ10 in the blend may be varying with M_n as a result of solution aggregation of low M_n PTQ10. Worth noting is the fact that the spectra reveal sharper peaks for high M_n PTQ10 indicating that the polymer in that case has a better defined and narrower absorption band. From the device point of view, the higher absorption allows the high M_n polymer to absorb light more effectively and this is, at least in part, responsible for the higher photocurrents obtained for blends containing high M_n PTQ10 (Figure 2).

The larger bandgap of PTQ10:IDIC solar cells makes the EQE reach up to 800 nm, instead of the 950 nm reached by Y-acceptor-based solar cells. It can also be seen that in the area where PTQ10 absorbs, the EQE is higher when Y-family acceptors are used, compared to cells including IDIC (**Figure 4a**). This is probably

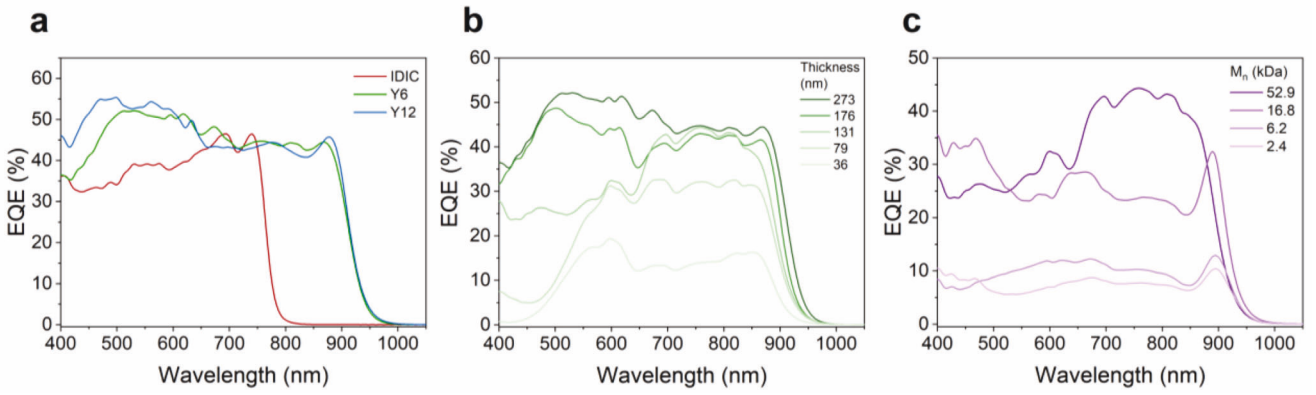

Figure 4. a) External Quantum Efficiency of the optimized devices of PTQ10:IDIC, PTQ10:Y6, and PTQ10:Y12 with PAL thickness 190, 302, and 339 nm, respectively ; b) of PTQ10 (M_n = 52.9 kDa):Y6 devices as a function of PAL thickness ; c) PTQ10:Y6 devices with similar PAL thickness and different PTQ10 molecular weight (ie. M_n = 2.4 kDa, M_n = 6.2 kDa, M_n = 16.8 kDa, and M_n = 52.9 kDa with PAL thickness 194, 182, 181, and 189 nm, respectively).

due to a thinner optimum thickness (Figure 2), which does not permit full absorption by the relatively low absorbing PTQ10.[75] The higher and more extended EQE for devices based on Y-derivatives agrees well with the higher photocurrent observed for these systems compared to those based on IDIC.

Regarding the PTQ10:Y6 system, with M_n = 52.9 kDa, there is an increase of the EQE in the PTQ10 absorption region when the PAL thickness increases, being much smaller than the Y6 contribution for thin PAL (Figure 4b). This is consistent with the absorption measurements, as shown in Figure 3. This panchromatic absorption contributes to the better photocurrent measured for thick films for devices based on high M_n PTQ10. On the other hand, Figure 4c shows the effect of PTQ10 molecular weight on EQE in PTQ10:Y6 solar cells with similar active layer thicknesses (between 181 and 194 nm). Higher M_n leads to improved EQE by allowing for more efficient absorption of light, in combination with improved charge transport (see below).

In order to elucidate the influence of the molecular weight variation of the PTQ10 donor polymer on the device physics, we measured PTQ10:Y6 solar cells as a function of light intensity. The main photovoltaic parameters as a function of light intensity are shown in Figure S5 (Supporting Information). The correlation between the V_{OC} and light intensity is a well-established qualitative approach to infer the dominant recombination mechanism in organic solar cells. Certainly, the light ideality factor (n) is calculated by fitting the measured V_{OC} as a function of light intensity (Φ) using the following equation:[83,84]

$$n = \frac{q}{k_B T} \frac{\mathrm{d}V_{OC}}{\mathrm{d}\ln\Phi} \quad (1)$$

with q being the elementary charge, T the temperature, and k_B the Boltzmann constant. When the bimolecular recombination is strongly dominant, a factor n close to unity is expected. In contrast, when bulk traps are present in the PAL, promoting trap-assisted recombination, an increase of n is observed. The n factor of PTQ10:Y6 solar cells with different M_n of PTQ10 as a function of PAL thickness is depicted in **Figure 5**. The ideality factor is closer of unity when the M_n is higher, and typically higher than 1.2 for the samples with low M_n. The observed increase in the ideality factor indicates a correlation between the molecular weight of PTQ10 and the number of traps present in the active layer. Specifically, lower molecular weight of PTQ10 is associated with a higher number of traps in the active layer. As expected, solar cells with medium and low PTQ10 M_n show an increment of the ideality factor with the PAL thickness. The ideality factor of solar cells with high PTQ10 M_n is closer to the unit than solar cells with low and medium PTQ10 M_n.

We next characterize the charge transport properties of each material by fabricating organic field effect transistors (OFETs). Representative output characteristics of PTQ10, IDIC, Y6, and Y12 based OFETs are shown in Figure S6 (Supporting Information). The charge carrier mobility values have been extracted from the transfer characteristics measurements in the saturation regime (Figure S7, Supporting Information), and the values are summarized in **Table 1**. The hole mobility of PTQ10 polymer increases progressively from $(1.76 \pm 0.55)\cdot10^{-4}$ to $(2.45 \pm 0.43)\cdot10^{-3}$ $cm^2\ V^{-1}\ s^{-1}$ when increasing the M_n from 2.4 to 54.4 kDa, respectively. This increase by more than one order of magnitude is likely

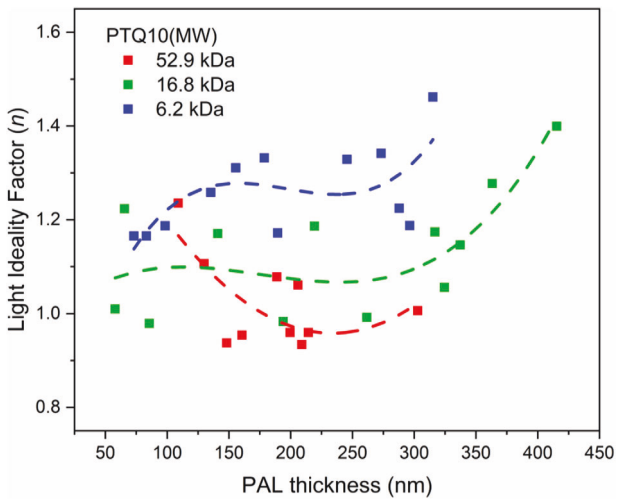

Figure 5. Light ideality factor (n) of PTQ10:Y6 solar cells with PTQ10 low (M_n = 6.2 kDa), medium (M_n = 16.8 kDa), and high (M_n = 52.9 kDa) molecular weight. Dashed lines represent polynomial fits to the data, serving as visual guides.

Table 1. Field effect mobility values of the organic semiconductors used in this work. The average value was extracted from the transfer characteristics of 8 OFETs for each material, and the error is the corresponding standard deviation.

Material	Mobility [$cm^2\ V^{-1}\ s^{-1}$]
PTQ10 M_n = 2.4 kDa	$(1.76 \pm 0.55)\cdot10^{-4}$
PTQ10 M_n = 6.2 kDa	$(1.63 \pm 0.43)\cdot10^{-4}$
PTQ10 M_n = 16.8 kDa	$(1.40 \pm 0.30)\cdot10^{-3}$
PTQ10 M_n = 52.9 kDa	$(1.41 \pm 0.14)\cdot10^{-3}$
PTQ10 M_n = 54.4 kDa	$(2.45 \pm 0.43)\cdot10^{-3}$
IDIC	$(3.46 \pm 1.36)\cdot10^{-3}$
Y6	$(9.52 \pm 0.48)\cdot10^{-3}$
Y12	$(4.06 \pm 0.19)\cdot10^{-2}$

due to changes in microstructure that affect the interchain hopping rate (e.g., crystallinity) or intra-chain transport (e.g., through crystallite inter-connectivity). As degree of crystallinity typically decreases with increasing M_n, we expect that the most significant impact on mobility arises from the inter-crystallite connectivity granted by high M_n chains.[85] Long polymers can form interconnecting chains that act as bridges between individual crystallites, facilitating efficient charge transport and promoting higher mobility. We will come back to this point when looking at GIWAXS data.

PTQ10 OFETs with low M_n present a switch on voltage shifted to more negatives values (V_{ON} ~ −32 V) compared to those of higher M_n (V_{ON} ~ −15 V) (Figure S7, Supporting Information). A higher trap density, which are localized states in the energy bandgap of the semiconductor, can lead to a higher threshold voltage, since the V_{ON} of an OFET is strongly dependent on the density of traps present in the organic semiconductor.[86] Hence, our results point toward the fact that OFETs with lower M_n have more traps, which can trap charge carriers and is in agreement with the increase of the ideality factor of solar cells with low M_n (Figure 5). Our findings align with prior studies, confirming that charge transport in semiconducting polymers predominantly takes place along the polymer backbones and is restricted by interchain hopping, making extended crystallinity dispensable.[87,88] If the molecular weight is high enough, long polymer chains can connect ordered regions, interconnected network facilitated by tie-molecules, greatly improving charge transport in the film.[89] On the other hand, Y6 and Y12 OFETs show higher electron mobility than the values obtained with IDIC OFETs (Table 1). The mean mobility of Y12 OFETs is more than one order of magnitude higher than IDIC OFETs, $(4.06 \pm 0.19)\cdot10^{-2}$ and $(3.46 \pm 1.36)\cdot10^{-3}$, respectively, being the mobility of Y6 OFETs also higher than IDIC OFETs. High mobility values can lead to relatively high *FF* by reducing the losses due to recombination of charges. The mobility values obtained with the OFETs agree with the *FF* shown in Figure 2, where it can be observed that increasing the M_n of PTQ10 the *FF* also increases in the same direction as mobility does. It appears that a more balanced mobility helps the *FF*. The agreement between *FF* and mobilities extends to the different NFA. We argue that higher mobility values are also connected to the capability of the blend to maintain the PCE for thick PALs.

In order to gain a deeper insight on film morphology, the solid-state molecular packing of low and high molecular weight PTQ10, both as neat and blend films, was studied by grazing incidence wide-angle X-ray scattering (GIWAXS). In **Figure 6**, the 2D patterns obtained and their corresponding intensity profiles along the out-of-plane (OOP, z) and in-plane (IP, r) directions are shown. The complete set is shown in Figure S8 (Supporting Information). Pristine PTQ10 thin films with low M_n display sharper and better-defined diffraction peaks compared to high M_n films, which suggests a larger degree of structural order in the former. Moreover, while low-M_n films exhibit a preferred "edge-on" orientation of polymer molecules, a preferential "face-on" orientation is found in high M_n films.

The distinctive feature of the PTQ10:Y6 microstructure is its partially amorphous structure, which is in contrast to many BHJ. Instead, discernible narrow reflections persist, implying a substantial presence of structurally ordered domains and thus, chemical homogeneity within this BHJ. The patterns of the blend PTQ10:Y6 present an intense broad halo and both isotropic lamellar and pi–pi stacking reflections, with a "face-on" tendency of the latter one. The GIWAXS 1D line cuts corresponding to the in-plane (q_{xy}) and out-of-plane (q_z) scattering intensities are also shown in Figure 6c,d,g,h. It is observed that above 6.2 kDa, the polymer presents much less crystallinity and orientation (as proved by the isotropic reflections) (Figure S8, Supporting Information). For the blend case, a decrease of "lamellar" intensity in OOP and increase in IP is observed. This proves the increased of "face-on" stacking for high M_n.

The GIWAXS data inform us that the origin of the higher absorption for high M_n PTQ10 blends is not related to a higher density of dipoles but more likely due to improved vertical orientation of the pi–pi reflection, which can be attributed to higher chain orientation in the plane (more isotropic molecular distribution for the lower M_n batches).[82] Moreover, it confirms that the changes in mobility are more likely associated to better interchain connectivity.[85] More rigid backbones, like PTQ10 compared to P3HT, will lead to an increase in the critical molecular weight.

In the final set of experiments, we have focused on the stability of the different systems. We measured the thermal stability of OPV based on PTQ10:Y6 with different donor M_n by monitoring the performance of the solar cells after annealing them at several temperatures for 10 min from 85 °C to 265 °C with 15 °C steps. The whole set is shown in Figures S9–S12 (Supporting Information), while **Figure 7** summarizes the main parameters for the best performing device for each M_n. The results show relatively stable performances up to a temperature of 150 °C, after which both V_{OC} and J_{SC} plumped for low molecular weight. When the temperature reached 200 °C, the V_{OC} and J_{SC} for blends containing the 2.4 and 6.2 kDa batches are <20% the original value, while for higher M_n they are still ≈80% of the values for the unannealed sample. The strong drop in photocurrent for the high molecular weight samples happens at ≈250 °C. We should note, however, that cells are not fully stable up to that temperature but rather only more slowly changing. At that temperature, it is clearly understandable that there is a big drop in efficiency due to the morphological instability of the blend, triggered by Y6 with lower glass transition temperature.[90] Overall, these results indicate that high molecular weight organic solar cells are more

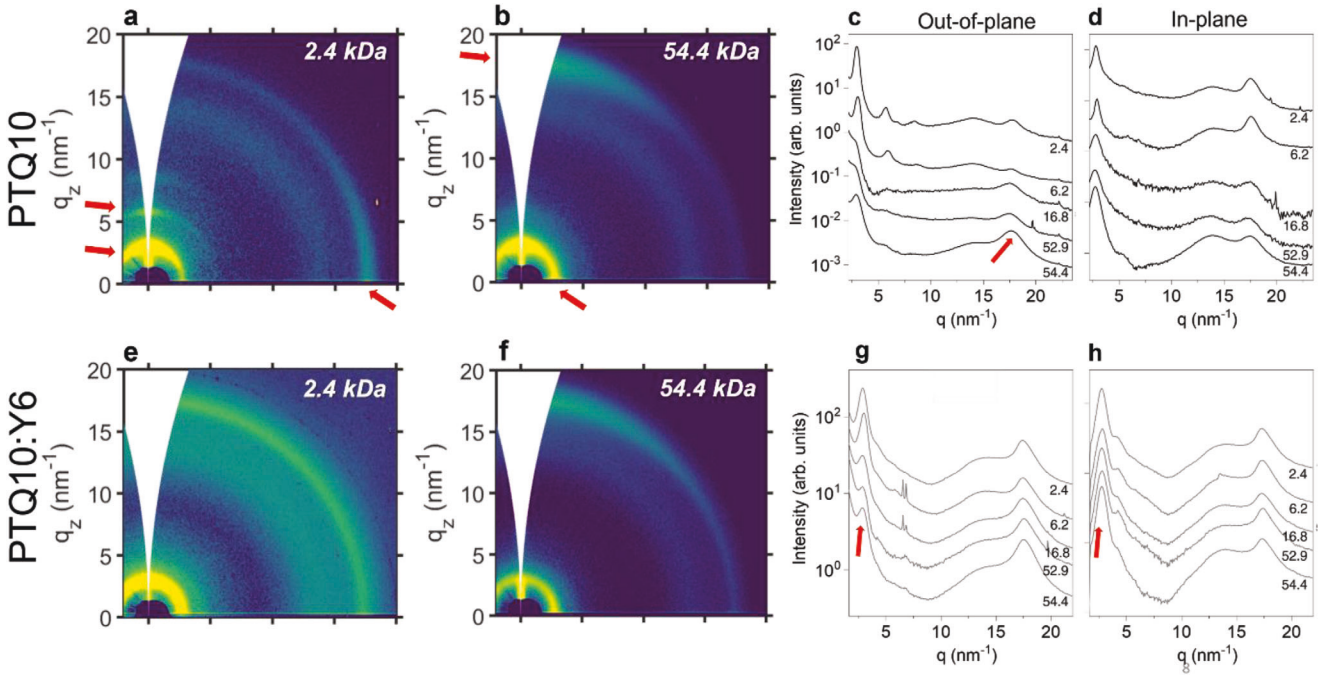

Figure 6. a–d) 2D GIWAXS data and line profiles in the out-of-plane and in-plane directions of PTQ10 and e–h)PTQ10:Y6 .

thermally stable, which is an important factor in determining the long-term performance and stability of these devices. These findings highlight the importance of optimizing the molecular weight of the organic material used in organic solar cells to enhance their thermal stability and long-term performance.

In order to further elucidate the origin of thermal stability differences on devices, we characterize the thermal properties of low and high M_n PTQ10 films. The glass transition temperature (T_g) was determined for 2.4 and 52.9 kDa PTQ10 solution processed films using two different methods based on fast scanning calorimetry (FSC), namely physical aging experiments[91,92] and temperature-modulated FSC experiments (see Supporting Information for details). Interestingly, a 15–25 °C shift on T_g was determined between 2.4 and 52.9 kDa with both methods (see Supporting information for more detail), higher for larger M_n. In the case of physical aging experiments (Figures S13 and S14, Supporting Information), we found a T_g = 181.6 °C for M_n = 2.4 kDa and a T_g = 195.3 °C for M_n = 52.9 kDa. For temperature modulated DSC (Figures S15–S17, Supporting Information), the transitions happen at ≈150 °C and 175 °C for M_n = 2.4 kDa and M_n = 52.9 kDa, respectively. Both techniques support the increase in glass transition temperature with molecular weight, and thus the improved thermal stability for the devices based on higher M_n PTQ10, in agreement with previous results for other systems.[93] Additionally, we confirm the thermal stability of PTQ10 by GIWAXS (Figure S18, Supporting Information). After annealing the film, we observe only minor variations in intensity for polymer crystals with edge-on orientation (out-of-plane direction), while no significant differences are observed in GIWAXS in-plane direction. Finally, Raman spectroscopic analysis was conducted on PTQ10:Y6 films annealed at high temperatures (200–260 °C). In Figure S19 (Supporting Information), the Raman spectra of these PTQ10:Y6 films are depicted, along with the Raman spectra of all organic semiconductors employed in this work. Slight variations in intensity were observed in the Raman spectroscopic profiles of low M_n PTQ10 samples, characterized by more constrained and pronounced spectral peaks, which can be related to a higher molecular order of the material by increasing the annealing temperature. Conversely, the Raman spectra of films comprising high M_n PTQ10 exhibited negligible dissimilarities under the aforementioned annealing conditions, and a spectral intensity notably superior than low M_n PTQ10, indicating an increase in the fraction of the polymer contributing to the Raman intensity.

3. Conclusion

In this work, we have evaluated the role of molecular weight donor polymer in PTQ10-based BHJ solar cells in terms of OPV performance, active layer thickness tolerance and thermal stability. We studied five different molecular weights (M_n = 2.4 – 54.4 kDa) of PTQ10 blended with three different NFAs, namely IDIC, Y6 and Y12. The photovoltaic performance increases with molecular weight for the three material combinations, mainly due to improved photocurrent and somehow *FF*. UV–vis and EQE measurements show that higher M_n leads to improved absorption and charge collection at the spectral range where PTQ10 absorbs. Mobility data, as extracted from OFETs, also shows an increase in hole mobility with M_n. This is not due to an improved crystallinity degree (as seen by GIWAXS), but probably due to an improvement in connectivity granted by the longer chains. On the other hand, the optimum film thickness appears to be larger and the PCE more thickness tolerant for high M_n donors.

Finally, thermal stability was also studied by accumulative thermal treatment of the devices based on PT10:Y6 from 85 °C to 265 °C. Performance evolution of devices under thermal stress

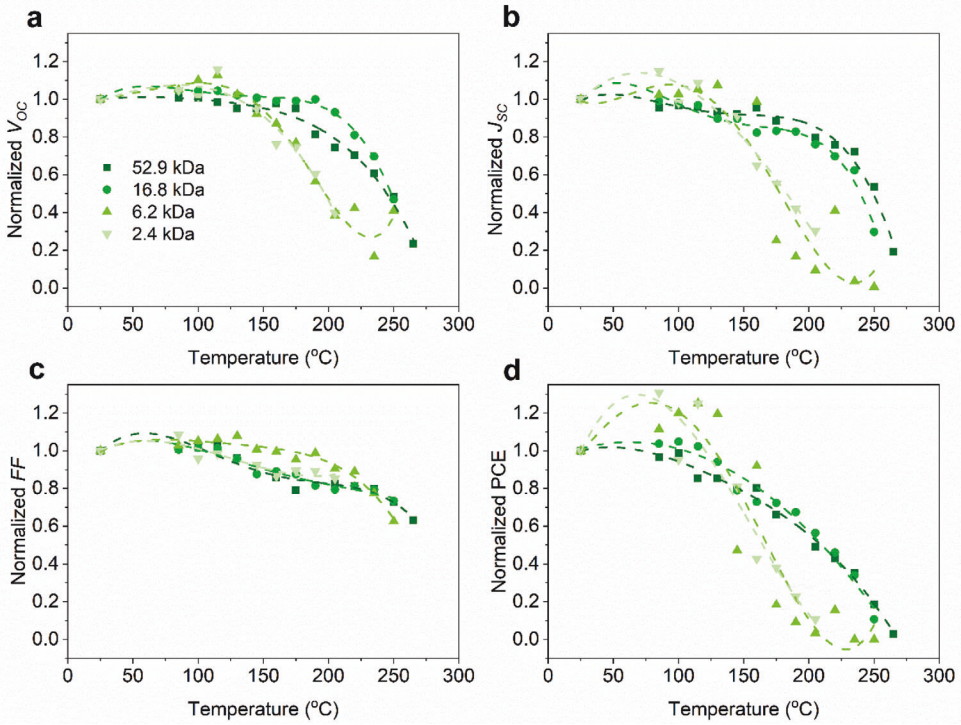

Figure 7. Main photovoltaic parameters of PTQ10:Y6 solar cells as a function of temperature annealing for different M_n of PTQ10. Dashed lines represent polynomial fits to the data, serving as visual guides.

show that high M_n OPVs were more stable. Moreover, a difference in glass temperature of 15 °C to 25 °C was found between 2.4 and 52.9 kDa PTQ10 films which explains, at least in part, the improved stability of cells based on higher M_n donor. Increasing molecular weight is, therefore, a good strategy to simultaneously improve efficiency, stability, and thickness tolerance. Our results support PTQ10 as a highly favorable polymer to push commercial applications of OPV forward. Although factors affecting the performance and stability of this novel low-cost material remain to be fully examined, our work highlight some important indications of practical utility for processability.

4. Experimental Section

Materials: All reagents and solvents were purchased from commercial sources and were used without further purification. Poly[[6,7-difluoro[(2-hexyldecyl)oxy]−5,8-quinoxalinediyl]−2,5-thiophenediyl] (PTQ10) with different molecular weight ranging from low (M_n = 2.4 kDa), medium (M_n = 16.8 kDa) and high (M_n = 52.9 and 54.4 kDa) molecular weight were provided by 1-Material. Another low molecular PTQ10 with M_n = 6.2 KDa was included in the study purchased from a different provider (Lumtec). 2,2′-[(4,4,9,9-Tetrahexyl-4,9-dihydro-s-indaceno[1,2-b:5,6-b′]-dithiophene-2,7-diyl)bis[methylidyne(3-oxo-1H-indene-2,1(3H)-diylidene)]]bis-propanedinitrile (IDIC), 2,2″-((2Z,2″Z)-((12,13-bis(2-ethylhexyl)−3,9-diundecyl-12,13-dihydro-[1,2,5]thiadiazolo[3,4-e]thieno[2“,3”:4′,5″]thieno[2″,3″:4,5]pyrrolo[3,2-g]thieno[2″,3″:4,5]thieno[3,2-b]indole-2,10-diyl)bis(methanylylidene))bis(5,6-difluoro-3-oxo-2,3-dihydro-1H-indene-2,1-diylidene))dimalononitrile (Y6) and 2,2″-((2Z,2″Z)-((12,13-bis(2-butyloctyl)−3,9-diundecyl-12,13-dihydro-[1,2,5]thiadiazolo[3,4-e]thieno[2″,3″:4′,5″]thieno[2″,3″:4,5]pyrrolo[3,2-g]thieno[2″,3″:4,5]thieno[3,2-b]indole-2,10-diyl)bis(methanylylidene))bis(5,6-difluoro-3-oxo-2,3-dihydro-1H-indene-2,1-diylidene))dimalononitrile (Y12) were purchased from 1-Material.

ZnO ink formulation (N-10) was purchased from Avantama. Molybdenum oxide (MoO_x) was acquired from Alfa Aesar. Chlorobenzene was purchased from Merck and used as received. The glass substrates with patterned indium tin oxide (ITO; 100 nm thick) were purchased from Ossila, allowing the fabrication of 24 devices in just one glass slide (75 mm × 25 mm).

Solar Cell Fabrication: The organic solar cell devices were fabricated with an inverted structure of ITO/ZnO/PTQ10: NFA/MoO_X/Ag, with different molecular weight (M_n) of PTQ10 and NFA was either IDIC, Y6 or Y12. The substrates were cleaned by consecutive sonication baths in acetone, Hellmanex 10 vol% solution in water, isopropanol (5 min each), and sodium hydroxide (NaOH) 10 vol% (10 min), and finally rinsing with deionized (DI) water. The ZnO, which acts as electron transport layer (ETL), was deposited using an automatic blade coater Zehntner ZAA 2300 with an aluminum applicator Zehntner ZUA 2000, in air conditions with a droplet volume of 50 µL, a blade gap of 150 µm, at a constant speed of 5 mm s^{-1} and the substrate temperature set at 40 °C. ETL layer was annealed at 100 °C for 10 min before transferring to a nitrogen-filled glovebox. The photoactive layer (PAL) was blade coated in the glovebox with a blade gap of 200 µm, at substrate temperature of 88 °C, and at decelerating speed from 90 to 10 mm·s^{-1} across the 75 mm-long direction providing a thickness-gradient layer. PTQ10:Y6, PTQ10:Y12, and PTQ10:IDIC blends, at weight ratio 1:1.5, were prepared for each M_n at 20 mg·mL^{-1} dissolved in chlorobenzene. Then, samples were annealed at 100 °C for 10 min. MoO_x (40 nm) and Ag (150 nm) layers were finally evaporated in an ultra-high vacuum at a rate of 0.5 and 1 Å s^{-1}, respectively.

Solar Cell Characterization: The *J–V* characteristics were automatically acquired in air using a Keithley 2400 source meter in combination with an Arduino-based multiplexer/switcher to measure of up to 24 devices in a row. A SAN-EI Electric, XES-100S1 AAA solar simulator was used as an AM1.5G illumination source with homogeneous illumination in a

10 cm × 10 cm area. The solar simulator was previously calibrated with a certified silicon solar cell (Oriel). Light intensity dependence measurements were carried out using mesh attenuation filters. The external quantum efficiency (EQE) measurement setup consists of homemade system that uses a Supercontinuum White laser (4 W, Fianium PM-SC) coupled to a Fianium monochromator (LLTFContrast), with the power controlled by a broad-band silicon photodetector (Thorlabs S120V 200–1100 nm 50 mW). The current was acquired using a Keithley 2450 SourceMeter. The sample is enclosed on a black box, to prevent any light from affecting the measurement. The EQE wavelength scan was from 400 to 1100 nm every 1 nm.

Field-Effect Transistor Fabrication and Measurement: A bottom-gate bottom-contact configuration was used in the fabrication of field-effect transistors. The substrates employed for solution coating consisted of Si/SiO_2 (200 nm SiO_2) from Si-Mat with photolithography patterned electrodes of 4 nm of Cr and 40 nm of gold, deposited by thermal evaporation. The channel width/length aspect ratio was set to 1000 (L = 100 and 50 µm). Substrates were cleaned via ultrasonication in acetone and isopropanol. Solutions of the organic semiconductor, dissolved in chlorobenzene (20 mg mL^{-1}), were blade coated in a nitrogen-filled glovebox at 20 mm s^{-1} and a substrate temperature of 88 °C. The electrical measurements were performed in glovebox using a Keithley 2612A and homemade MATLAB software connected to the samples with Everbeing tungsten probing tips.

Thin Film Characterization—Thickness: The film thickness was measured using a mechanical profilometer (Dektak 150, Bruker).

Thin Film Characterization—Raman spectroscopy: Samples were prepared by blade coating in PTQ10:Y6 solutions, prepared with the same conditions than for OPV and OFETs, on a glass substrate (75 mm × 25 mm) in a nitrogen-filled glovebox at 20 mm s^{-1} and a substrate temperature of 88 °C. Later, the samples were annealed in a Koffler bench with a controlled temperature gradient along the sample. The Raman measurements were acquired using a WiTec alpha 300 RA+ confocal Raman setup, coupled to an Olympus objective with 10X magnification (NA 0.25). A laser centred at 488 nm was employed.

Thin Film Characterization—UV–Vis Absorption Spectroscopy: UV–vis spectra were recorded with a Shimadzu UV-2550 spectrometer.

Thin Film Characterization—GIWAXS: GIWAXS measurements were carried out using small angle X-ray scattering system (ALBA Synchrotron, NCD SWEET beamline). The samples for the GIWAXS measurements were prepared on Si substrates using solutions of PTQ10:Y6 blends with the different molecular weight. Wavelength = 0.1 nm; Sample-to-detector distance = 200 mm; Rayonix (LX255-HS). Incidence angle = 0.12°.

Supporting Information

Supporting Information is available from the Wiley Online Library or from the author.

Acknowledgements

The authors are grateful to 1-Material for providing custom molecular weight PTQ10 polymer and for the fruitful discussions. S.R.-G. is thankful to the Marie Sklodowska-Curie Actions (H2020-MSCA-IF-2020) for grant agreement No. 101025608, IDEAL; for the financial support provided by Ajuntament de Barcelona and the Ministeri de Ciència i Innovació within the framework of Barcelona Capital Cultural i Científic, through the project Bus Stop Integrated Organic Photovoltaic (TERRA) (22S09542-001). The authors acknowledge Dr. Bernhard Dörling for building the electronic controller of the accelerated blade coater and Dr. M. Gibert-Roca for designing the corresponding multiplexor. M.C.-Q. thanks to the Spanish Ministry of Science and Innovation for funding through projects PID2021-128924OB-I00 and TED2021-131911B-I00. This work was supported by the MADRAS project funded from the European Union Horizon 2020 research and innovation programme under grant agreement No. 862492. This work was also funded by MCIN/AEI/10.13039/501100011033/ERDF,UE with projects GENESIS PID2019-111682RB-I00 and SENSATION PID2022-141393OB-I00, and through the "Severo Ochoa" Programme for Centers of Excellence in R&D (FUNFUTURE CEX2019-000917-S).

Conflict of Interest

The authors declare no conflict of interest.

Data Availability Statement

The data that support the findings of this study are available from the corresponding author upon reasonable request.

Keywords

molecular weight, organic photovoltaics, stability, thickness tolerance, upscaling

Received: December 27, 2023
Revised: January 10, 2024
Published online: January 26, 2024

[1] R. Xue, J. Zhang, Y. Li, Y. Li, *Small* **2018**, *14*, 1801793.
[2] Y. Hu, J. Wang, C. Yan, P. Cheng, *Nat. Rev. Mater.* **2022**, *7*, 836.
[3] Y. Li, X. Huang, H. K. M. Sheriff, S. R. Forrest, *Nat. Rev. Mater.* **2022**, *8*, 186.
[4] X. Rodríguez-Martínez, S. Riera-Galindo, L. E. Aguirre, M. Campoy-Quiles, H. Arwin, O. Inganäs, *Adv. Funct. Mater.* **2022**, *33*, 2213220.
[5] Y. Cui, Y. Xu, H. Yao, P. Bi, L. Hong, J. Zhang, Y. Zu, T. Zhang, J. Qin, J. Ren, Z. Chen, C. He, X. Hao, Z. Wei, J. Hou, *Adv. Mater.* **2021**, *33*, 2102420.
[6] L. Zhu, M. Zhang, J. Xu, C. Li, J. Yan, G. Zhou, W. Zhong, T. Hao, J. Song, X. Xue, Z. Zhou, R. Zeng, H. Zhu, C.-C. Chen, R. C. I. MacKenzie, Y. Zou, J. Nelson, Y. Zhang, Y. Sun, F. Liu, *Nat. Mater.* **2022**, *21*, 656.
[7] K. Chong, X. Xu, H. Meng, J. Xue, L. Yu, W. Ma, Q. Peng, *Adv. Mater.* **2022**, *34*, 2109516.
[8] C. He, Y. Pan, Y. Ouyang, Q. Shen, Y. Gao, K. Yan, J. Fang, Y. Chen, C.-Q. Ma, J. Min, C. Zhang, L. Zuo, H. Chen, *Energy Environ. Sci.* **2022**, *15*, 2537.
[9] Y. Jiang, X. Dong, L. Sun, T. Liu, F. Qin, C. Xie, P. Jiang, L. Hu, X. Lu, X. Zhou, W. Meng, N. Li, C. J. Brabec, Y. Zhou, *Nat. Energy* **2022**, *7*, 352.
[10] L. Zhan, S. Li, Y. Li, R. Sun, J. Min, Y. Chen, J. Fang, C. Ma, G. Zhou, H. Zhu, L. Zuo, H. Qiu, S. Yin, H. Chen, *Adv. Energy Mater.* **2022**, *12*, 2201076.
[11] H. Lu, W. Liu, G. Ran, Z. Liang, H. Li, N. Wei, H. Wu, Z. Ma, Y. Liu, W. Zhang, X. Xu, Z. Bo, *Angew. Chem., Int. Ed.* **2023**, *62*, e202314420.
[12] W. R. Mateker, M. D. McGehee, *Adv. Mater.* **2017**, *29*, 1603940.
[13] C. J. Brabec, A. Distler, X. Du, H. Egelhaaf, J. Hauch, T. Heumueller, N. Li, *Adv. Energy Mater.* **2020**, *10*, 2001864.
[14] F. Zhao, H. Zhang, R. Zhang, J. Yuan, D. He, Y. Zou, F. Gao, *Adv. Energy Mater.* **2020**, *10*, 2002746.
[15] Z. Jiang, F. Wang, K. Fukuda, A. Karki, W. Huang, K. Yu, T. Yokota, K. Tajima, T.-Q. Nguyen, T. Someya, *Proc. Natl. Acad. Sci. U. S. A.* **2020**, *117*, 6391.
[16] Y. Liang, D. Zhang, Z. Wu, T. Jia, L. Lüer, H. Tang, L. Hong, J. Zhang, K. Zhang, C. J. Brabec, N. Li, F. Huang, *Nat. Energy* **2022**, *7*, 1180.
[17] I. Burgués-Ceballos, M. Stella, P. Lacharmoise, E. Martínez-Ferrero, *J. Mater. Chem. A* **2014**, *2*, 17711.

[18] L. Duan, A. Uddin, *Adv. Sci.* **2020**, *7*, 1903259.
[19] M. Riede, D. Spoltore, K. Leo, *Adv. Energy Mater.* **2021**, *11*, 2002653.
[20] G. Bernardo, T. Lopes, D. G. Lidzey, A. Mendes, *Adv. Energy Mater.* **2021**, *11*, 2100342.
[21] G. Zhang, F. R. Lin, F. Qi, T. Heumüller, A. Distler, H.-J. Egelhaaf, N. Li, P. C. Y. Chow, C. J. Brabec, A. K.-Y. Jen, H.-L. Yip, *Chem. Rev.* **2022**, *122*, 14180.
[22] L. Ye, M. Gao, J. Hou, *Sci. China: Chem.* **2021**, *64*, 1875.
[23] B. Lin, X. Zhou, H. Zhao, J. Yuan, K. Zhou, K. Chen, H. Wu, R. Guo, M. A. Scheel, A. Chumakov, S. V. Roth, Y. Mao, L. Wang, Z. Tang, P. Müller-Buschbaum, W. Ma, *Energy Environ. Sci.* **2020**, *13*, 2467.
[24] Y. Wang, J. Lee, X. Hou, C. Labanti, J. Yan, E. Mazzolini, A. Parhar, J. Nelson, J. Kim, Z. Li, *Adv. Energy Mater.* **2021**, *11*, 2003002.
[25] S. H. K. Paleti, S. Hultmark, J. Han, Y. Wen, H. Xu, S. Chen, E. Järsvall, I. Jalan, D. R. Villalva, A. Sharma, J. I. Khan, E. Moons, R. Li, L. Yu, J. Gorenflot, F. Laquai, C. Müller, D. Baran, *Nat. Commun.* **2023**, *14*, 4608.
[26] P. Jiang, L. Hu, L. Sun, Z. Li, H. Han, Y. Zhou, *Chem. Sci.* **2022**, *13*, 4714.
[27] J. Gao, J. Wang, C. Xu, Z. Hu, X. Ma, X. Zhang, L. Niu, J. Zhang, F. Zhang, *Sol. RRL* **2020**, *4*, 2000364.
[28] Y.-J. Cheng, C.-H. Hsieh, P.-J. Li, C.-S. Hsu, *Adv. Funct. Mater.* **2011**, *21*, 1723.
[29] Y.-C. Chao, C.-H. Chuang, H.-L. Hsu, H.-J. Wang, Y.-C. Hsu, C.-P. Chen, R.-J. Jeng, *Sol. Energy Mater. Sol. Cells* **2016**, *157*, 666.
[30] L. Tan, F. Yang, M. R. Kim, P. Li, D. T. Gangadharan, J. Margot, R. Izquierdo, M. Chaker, D. Ma, *ACS Appl. Mater. Interfaces* **2017**, *9*, 26257.
[31] W. Yang, Z. Luo, R. Sun, J. Guo, T. Wang, Y. Wu, W. Wang, J. Guo, Q. Wu, M. Shi, H. Li, C. Yang, J. Min, *Nat. Commun.* **2020**, *11*, 1218.
[32] Q. Qi, K. Xian, H. Ke, J. Wu, K. Zhou, M. Gao, J. Liu, S. Li, W. Zhao, Z. Chen, L. Ye, *ACS Appl. Energy Mater.* **2022**, *5*, 15656.
[33] K. Xian, S. Zhang, Y. Xu, J. Liu, K. Zhou, Z. Peng, M. Li, W. Zhao, Y. Chen, Z. Fei, J. Hou, Y. Geng, L. Ye, *Sci. China: Chem.* **2023**, *66*, 202.
[34] M. Gao, K. Zhang, C. He, H. Jiang, X. Li, Q. Qi, K. Zhou, Y. Chen, W. Zhao, L. Ye, *Aggregate* **2022**, *4*, e289.
[35] G. Griffini, J. D. Douglas, C. Piliego, T. W. Holcombe, S. Turri, J. M. J. Fréchet, J. L. Mynar, *Adv. Mater.* **2011**, *23*, 1660.
[36] W. Feng, Z. Lin, J. Cui, W. Lv, W. Wang, Q. Ling, *Sol. Energy Mater. Sol. Cells* **2019**, *200*, 109982.
[37] H. D. Chau, S. H. Park, S. H. Jung, J. Y. Park, M. J. Kang, A. K. Harit, H. Y. Woo, M. J. Cho, D. H. Choi, *J. Mater. Chem. A* **2023**, *11*, 8719.
[38] L. Su, H. Huang, Y. Lin, G. Chen, W. Chen, W. Chen, L. Wang, C. Chueh, *Adv. Funct. Mater.* **2021**, *31*, 2005753.
[39] K. Ding, Y. Li, S. R. Forrest, *ACS Appl. Mater. Interfaces* **2022**, *14*, 5692.
[40] M. Kim, S. Park, D. Y. Ryu, K. Kim, *Polymer* **2016**, *103*, 132.
[41] F. Deledalle, T. Kirchartz, M. S. Vezie, M. Campoy-Quiles, P. Shakya Tuladhar, J. Nelson, J. R. Durrant, *Phys. Rev. X* **2015**, *5*, 011032.
[42] H. Zhou, L. Yang, W. You, *Macromolecules* **2012**, *45*, 607.
[43] H. Wu, C. Yang, Q. Li, N. B. Kolhe, X. Strakosas, M. Stoeckel, Z. Wu, W. Jin, M. Savvakis, R. Kroon, D. Tu, H. Y. Woo, M. Berggren, S. A. Jenekhe, S. Fabiano, *Adv. Mater.* **2022**, *34*, 2106235.
[44] S. E. Yoon, B. Kim, S. Y. Chun, S. Y. Lee, D. Jeon, M. Kim, S. Lee, B. E. Seo, K. S. Choi, F. S. Kim, T. Kim, H. Seo, K. Kwak, J. H. Kim, B. Kim, *Adv. Funct. Mater.* **2022**, *32*, 2202929.
[45] Q. Liu, S. Smeets, S. Mertens, Y. Xia, A. Valencia, J. D'Haen, W. Maes, K. Vandewal, *Joule* **2021**, *5*, 2365.
[46] L. Ye, S. Li, X. Liu, S. Zhang, M. Ghasemi, Y. Xiong, J. Hou, H. Ade, *Joule* **2019**, *3*, 443.
[47] A. Karki, J. Vollbrecht, A. J. Gillett, S. S. Xiao, Y. Yang, Z. Peng, N. Schopp, A. L. Dixon, S. Yoon, M. Schrock, H. Ade, G. N. M. Reddy, R. H. Friend, T.-Q. Nguyen, *Energy Environ. Sci.* **2020**, *13*, 3679.
[48] A. Wadsworth, Z. Hamid, M. Bidwell, R. S. Ashraf, J. I. Khan, D. H. Anjum, C. Cendra, J. Yan, E. Rezasoltani, A. A. Y. Guilbert, M. Azzouzi, N. Gasparini, J. H. Bannock, D. Baran, H. Wu, J. C. de Mello, C. J. Brabec, A. Salleo, J. Nelson, F. Laquai, I. McCulloch, *Adv. Energy Mater.* **2018**, *8*, 1801001.
[49] S. F. Hoefler, T. Rath, N. Pastukhova, E. Pavlica, D. Scheunemann, S. Wilken, B. Kunert, R. Resel, M. Hobisch, S. Xiao, G. Bratina, G. Trimmel, *J. Mater. Chem. A* **2018**, *6*, 9506.
[50] J. W. Kingsley, P. P. Marchisio, H. Yi, A. Iraqi, C. J. Kinane, S. Langridge, R. L. Thompson, A. J. Cadby, A. J. Pearson, D. G. Lidzey, R. A. L. Jones, A. J. Parnell, *Sci. Rep.* **2014**, *4*, 5286.
[51] W. Ma, G. Yang, K. Jiang, J. H. Carpenter, Y. Wu, X. Meng, T. McAfee, J. Zhao, C. Zhu, C. Wang, H. Ade, H. Yan, *Adv. Energy Mater.* **2015**, *5*, 1501400.
[52] Z. Ding, J. Kettle, M. Horie, S. W. Chang, G. C. Smith, A. I. Shames, E. A. Katz, *J. Mater. Chem. A* **2016**, *4*, 7274.
[53] J. Subbiah, B. Purushothaman, M. Chen, T. Qin, M. Gao, D. Vak, F. H. Scholes, X. Chen, S. E. Watkins, G. J. Wilson, A. B. Holmes, W. W. H. Wong, D. J. Jones, *Adv. Mater.* **2015**, *27*, 702.
[54] B. Fan, L. Ying, Z. Wang, B. He, X.-F. Jiang, F. Huang, Y. Cao, *Energy Environ. Sci.* **2017**, *10*, 1243.
[55] S. Chen, Y. An, G. K. Dutta, Y. Kim, Z.-G. Zhang, Y. Li, C. Yang, *Adv. Funct. Mater.* **2017**, *27*, 1603564.
[56] Z. Li, W. Zhong, L. Ying, F. Liu, N. Li, F. Huang, Y. Cao, *Nano Energy* **2019**, *64*, 103931.
[57] A. Zeng, X. Ma, M. Pan, Y. Chen, R. Ma, H. Zhao, J. Zhang, H. K. Kim, A. Shang, S. Luo, I. C. Angunawela, Y. Chang, Z. Qi, H. Sun, J. Y. L. Lai, H. Ade, W. Ma, F. Zhang, H. Yan, *Adv. Funct. Mater.* **2021**, *31*, 2102413.
[58] N. Schopp, S. Sabury, T. Chaney, J. Zhang, H. Wakidi, B. M. Kim, R. Sankar, H. M. Luong, P. Therdkatanyuphong, V. V. Brus, S. Marder, M. F. Toney, J. R. Reynolds, T.-Q. Nguyen, *ACS Energy Lett.* **2023**, *8*, 3307.
[59] B. Zheng, Y. Yue, J. Ni, X. Zhou, Y. He, X. Gui, H. Shen, Y. Jing, J. Zhao, J. Zhang, Y. Zhang, J. Wang, L. Jiang, L. Huo, *Adv. Funct. Mater.* **2023**, *33*, 2300981.
[60] C. Sun, F. Pan, H. Bin, J. Zhang, L. Xue, B. Qiu, Z. Wei, Z.-G. Zhang, Y. Li, *Nat. Commun.* **2018**, *9*, 743.
[61] Y. Wang, J. Luke, A. Privitera, N. Rolland, C. Labanti, G. Londi, V. Lemaur, D. T. W. Toolan, A. J. Sneyd, S. Jeong, D. Qian, Y. Olivier, L. Sorace, J.-S. Kim, D. Beljonne, Z. Li, A. J. Gillett, *Joule* **2023**, *7*, 810.
[62] Y. Wu, Y. Zheng, H. Yang, C. Sun, Y. Dong, C. Cui, H. Yan, Y. Li, *Sci. China: Chem.* **2020**, *63*, 265.
[63] N. Gasparini, M. Salvador, T. Heumueller, M. Richter, A. Classen, S. Shrestha, G. J. Matt, S. Holliday, S. Strohm, H.-J. Egelhaaf, A. Wadsworth, D. Baran, I. McCulloch, C. J. Brabec, *Adv. Energy Mater.* **2017**, *7*, 1701561.
[64] L. Hong, H. Yao, Z. Wu, Y. Cui, T. Zhang, Y. Xu, R. Yu, Q. Liao, B. Gao, K. Xian, H. Y. Woo, Z. Ge, J. Hou, *Adv. Mater.* **2019**, *31*, 1903441.
[65] W. Wang, Q. Wu, R. Sun, J. Guo, Y. Wu, M. Shi, W. Yang, H. Li, J. Min, *Joule* **2020**, *4*, 1070.
[66] Y. Shen, L. Liang, S. Zhang, D. Huang, J. Zhang, S. Xu, C. Liang, W. Xu, *Nanoscale* **2018**, *10*, 1622.
[67] B. Fan, K. Zhang, X.-F. Jiang, L. Ying, F. Huang, Y. Cao, *Adv. Mater.* **2017**, *29*, 1606396.
[68] R. Po, G. Bianchi, C. Carbonera, A. Pellegrino, *Macromolecules* **2015**, *48*, 453.
[69] E. Pascual-San-José, X. Rodríguez-Martínez, R. Adel-Abdelaleim, M. Stella, E. Martínez-Ferrero, M. Campoy-Quiles, *J. Mater. Chem. A* **2019**, *7*, 20369.
[70] X. Rodríguez-Martínez, E. Pascual-San-José, Z. Fei, M. Heeney, R. Guimerà, M. Campoy-Quiles, *Energy Environ. Sci.* **2021**, *14*, 986.
[71] A. Sánchez-Díaz, X. Rodríguez-Martínez, L. Córcoles-Guija, G. Mora-Martín, M. Campoy-Quiles, *Adv. Electron. Mater.* **2018**, *4*, 1700477.
[72] Fabrication of organic solar cells with thickness gradients – Nanopto Hands-On, https://nanopto.icmab.es/fabrication-of-organic-solar-

cells-with-thickness-gradients-nanopto-hands-on/ (accessed: 22 December 2023).
[73] Y. Lin, Q. He, F. Zhao, L. Huo, J. Mai, X. Lu, C.-J. Su, T. Li, J. Wang, J. Zhu, Y. Sun, C. Wang, X. Zhan, *J. Am. Chem. Soc.* **2016**, *138*, 2973.
[74] J. Yuan, Y. Zhang, L. Zhou, G. Zhang, H.-L. Yip, T.-K. Lau, X. Lu, C. Zhu, H. Peng, P. A. Johnson, M. Leclerc, Y. Cao, J. Ulanski, Y. Li, Y. Zou, *Joule* **2019**, *3*, 1140.
[75] X. Rodríguez-Martínez, S. Riera-Galindo, J. Cong, T. Österberg, M. Campoy-Quiles, O. Inganäs, *J. Mater. Chem. A* **2022**, *10*, 10768.
[76] F. Yang, Y. Huang, Y. Li, Y. Li, *npj Flexible Electron.* **2021**, *5*, 30.
[77] D. Zhang, B. Fan, L. Ying, N. Li, C. J. Brabec, F. Huang, Y. Cao, *SusMat* **2021**, *1*, 4.
[78] H. Choi, S.-J. Ko, T. Kim, P.-O. Morin, B. Walker, B. H. Lee, M. Leclerc, J. Y. Kim, A. J. Heeger, *Adv. Mater.* **2015**, *27*, 3318.
[79] J. Wu, J. Luke, H. K. H. Lee, P. Shakya Tuladhar, H. Cha, S.-Y. Jang, W. C. Tsoi, M. Heeney, H. Kang, K. Lee, T. Kirchartz, J.-S. Kim, J. R. Durrant, *Nat. Commun.* **2019**, *10*, 5159.
[80] W. Gao, Q. An, M. Hao, R. Sun, J. Yuan, F. Zhang, W. Ma, J. Min, C. Yang, *Adv. Funct. Mater.* **2020**, *30*, 1908336.
[81] M. S. Vezie, S. Few, I. Meager, G. Pieridou, B. Dörling, R. S. Ashraf, A. R. Goñi, H. Bronstein, I. McCulloch, S. C. Hayes, M. Campoy-Quiles, J. Nelson, *Nat. Mater.* **2016**, *15*, 746.
[82] K. Koynov, A. Bahtiar, T. Ahn, R. M. Cordeiro, H.-H. Hörhold, C. Bubeck, *Macromolecules* **2006**, *39*, 8692.
[83] S. R. Cowan, A. Roy, A. J. Heeger, *Phys. Rev. B* **2010**, *82*, 245207.
[84] C. M. Proctor, M. Kuik, T.-Q. Nguyen, *Prog. Polym. Sci.* **2013**, *38*, 1941.
[85] F. P. V. Koch, J. Rivnay, S. Foster, C. Müller, J. M. Downing, E. Buchaca-Domingo, P. Westacott, L. Yu, M. Yuan, M. Baklar, Z. Fei, C. Luscombe, M. A. McLachlan, M. Heeney, G. Rumbles, C. Silva, A. Salleo, J. Nelson, P. Smith, N. Stingelin, *Prog. Polym. Sci.* **2013**, *38*, 1978.
[86] S. Olthof, S. Singh, S. K. Mohapatra, S. Barlow, S. R. Marder, B. Kippelen, A. Kahn, *Appl. Phys. Lett.* **2012**, *101*, 253303.
[87] S. Himmelberger, K. Vandewal, Z. Fei, M. Heeney, A. Salleo, *Macromolecules* **2014**, *47*, 7151.
[88] S. Wang, S. Fabiano, S. Himmelberger, S. Puzinas, X. Crispin, A. Salleo, M. Berggren, *Proc. Natl. Acad. Sci. U. S. A.* **2015**, *112*, 10599.
[89] R. Noriega, J. Rivnay, K. Vandewal, F. P. V. Koch, N. Stingelin, P. Smith, M. F. Toney, A. Salleo, *Nat. Mater.* **2013**, *12*, 1038.
[90] Y. Qin, N. Balar, Z. Peng, A. Gadisa, I. Angunawela, A. Bagui, S. Kashani, J. Hou, H. Ade, *Joule* **2021**, *5*, 2129.
[91] J. Martín, N. Stingelin, D. Cangialosi, *J. Phys. Chem. Lett.* **2018**, *9*, 990.
[92] S. Marina, N. P. Kaufmann, A. Karki, E. Gutiérrez-Meza, E. Gutiérrez-Fernández, J. Vollbrecht, E. Solano, B. Walker, J. H. Bannock, J. De Mello, C. Silva, T. Nguyen, D. Cangialosi, N. Stingelin, J. Martín, *Adv. Mater.* **2020**, *32*, 2005241.
[93] C. Müller, E. Wang, L. M. Andersson, K. Tvingstedt, Y. Zhou, M. R. Andersson, O. Inganäs, *Adv. Funct. Mater.* **2010**, *20*, 2124.